JOURNAL OF APPLIED ELECTROCHEMISTRY 23 (1993) 1011–1016

Mechanism of the reverse dissolution of zinc in the presence of nickel
Part I: Influence of anodic products and substrate purity

C. CACHET, R. WIART

UPR15 du CNRS 'Physique des Liquides et Electrochimie' Tour 22, 4 place Jussieu, 75252 Paris, Cedex 05, France

I. IVANOV, S. RASHKOV

Institute of Physical Chemistry, Bulgarian Academy of Sciences, Sofia 1040, Bulgaria

Received 3 October 1992; revised 8 February 1993

From galvanostatic potential–time curves, voltammograms and impedance measurements, it is shown that the destabilization of the zinc deposition process by Ni^{2+} ions present in the acidic sulphate electrolyte is considerably favoured in the absence of a diaphragm separating the anode and cathode compartments. It is concluded that the deleterious influence of Ni^{2+} ions is enhanced by the anodically formed products which interfere with the slow interfacial processes taking place at the cathode surface. A stronger synergetic influence of nickel and oxidized species is demonstrated when using an aluminium cathode containing Fe impurities.

1. Introduction

The processes involved in zinc electrodeposition are highly sensitive to the presence of organic or mineral impurities [1] either added to the electrolyte or possibly generated during the electrolysis. For instance, in alkaline zincate electrolytes, the use of a soluble zinc anode gives rise to a progressive decrease in the cathode polarization during the zinc deposit growth, under galvanostatic conditions. Correlatively, both a change in the electrode impedance and the formation of spongy deposits have been observed [2], thus indicating that the electrode kinetics are strongly influenced by the presence of anodically dissolved zinc in the electrolyte.

With the highly acidic electrolytes used in zinc electrometallurgy, trace lead in zinc electrodeposits is inevitable since either silver–lead or pure lead anodes are employed in the electrowinning step [3, 4]. Trace lead modifies the morphology and crystal orientation of zinc deposits and it influences the coulombic efficiency of deposition [4].

The contamination of deposits by anodically dissolved metals can be avoided with the use of an insoluble platinum anode [5]. Also a diaphragm can be placed between the two electrodes [4] and this method has been used in chloride electrolytes so as to separate the chlorine evolved at the anode [6].

In highly acidic sulphate electrolytes, the kinetics of zinc deposition have been extensively investigated on the basis of electron microscopy, cyclic voltammetry and current efficiency [7–11]. It has been shown that the hydrogen discharge reaction is (i) inhibited by the presence of Zn^{2+} ions in the electrolyte, (ii) activated by the presence of nickel impurities in the electrolyte and (iii) sensitive to substrate impurities.

Recently, it has been shown from impedance measurements and potentiostatic polarization curves that zinc deposition normally occurs when hydrogen evolution is passivated on the deposit surface [12, 13]. Then the depassivation process is facilitated by the presence of nickel impurities in the electrolyte, leading to the deposit redissolution. Furthermore, the addition of hydrogen dioxide to the electrolyte considerably enhances hydrogen evolution [13]. These results suggest that the interactions between adsorbed nickel and oxidized adsorbates, formed on the zinc electrode near the corrosion potential, favour the destabilization of zinc deposition.

In the present work, with the use of a diaphragm, the influence of anodic products dissolved at a platinum anode has been investigated with regard to the deleterious effect of nickel impurities.

2. Experimental details

2.1. *Electrodes and cell*

The electrolysis cell, thermostated at 38° C, is depicted in Fig. 1. To separate the anode from the cathode, a Nafion® diaphragm (Dupont de Nemours) of 2 cm diameter was tightly fitted between a Teflon holder and a glass container screwed together. The volume of electrolyte contained within each separate compartment was about 200 cm^3. Holes were made in the Teflon holder to facilitate ion migration inside the anode compartment. When the diaphragm was used, the cathode and the reference electrode were placed

0021-891X

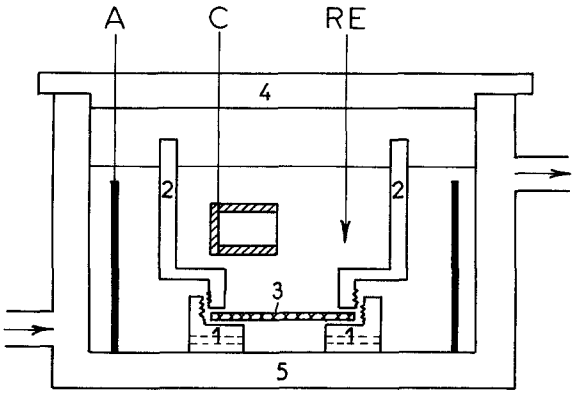

Fig. 1. Electrolysis cell with separate compartments: (1) Teflon holder; (2) glass container; (3) Nafion® diaphragm; (4) Teflon cap; (5) thermostated water in circulation. (RE) Reference electrode (C) cathode (A) anode.

in the inner compartment. Two different cathodes were successively used, whose effective surfaces were vertical and parallel to the symmetry axis of the cell, and they were insulated with epoxide resin (Buehler). A pure aluminum cathode, of effective surface area 0.2 cm^2, was fashioned from a 0.5 cm diameter cylinder (Johnson–Matthey, specpure). The second cathode, of effective surface area 0.1 cm^2, was prepared from a sheet of aluminium supplied by Riedel de Haën (RdH), of purity about 99.6% and containing several alloying elements, most commonly Fe, Cu, Zn, Si, Pb, Mn, etc..., the iron content being approximately 0.2% [11]. Before electrolysis, the cathode surface was polished with emery paper (grit 1200). The reference electrode consisted of a mercury/mercurous sulphate electrode in saturated potassium sulphate (SSE), used with two compartments separated by fitted glass. The counter electrode, placed in the outer compartment of the cell, was a platinum gauze cylinder.

2.2. *Electrolyte*

The solution was made of 50 g dm^{-3} zinc from $ZnSO_4.7H_2O$ and 120 g dm^{-3} H_2SO_4. To this solution, nickel was added as $NiSO_4.6H_2O$ at concentrations between 5 and 30 mg dm^{-3}. All chemicals were Merck products of analytical grade purity and the water was doubly ion-exchanged and twice distilled in a quartz apparatus.

2.3. *Experimental methods*

The potential–time $U(t)$ curves were obtained at constant current, the electrode potential U being sampled using a digital voltmeter (Keithley) at a frequency of 1 Hz. The data were stored in a microcomputer (IBM PS2) at a rate which was determined by the slope of the potential–time variation, and finally they were saved every two hours on microdisks. On average, about 250 to 300 points were saved in each period of two hours, thus allowing the potential–time variation to be easily followed for more than 100 h.

The voltammograms were obtained with a digital-analogue converter programmed to produce a scan rate of 3 mV s^{-1}.

Impedance measurements were performed using a frequency response analyser (Solartron 1174) controlled by an Apple II microcomputer.

3. Results and discussion

3.1. *Potential–time dependence*

In the presence of Ni^{2+} ions in the electrolyte, the potential–time curves recorded under galvanostatic conditions exhibit repetitive cycles of deposition/dissolution of zinc. Each cycle is characterized by an induction period defined by the time-lapse from the beginning of zinc deposition up to the sharp decrease in cathodic polarization corresponding to the reverse dissolution of zinc deposit. At 50 mA cm^{-2}, the variation of this induction period with the cycle number is shown in Fig. 2.

With 30 mg dm^{-3} Ni^{2+} in the electrolyte (Fig. 2a),

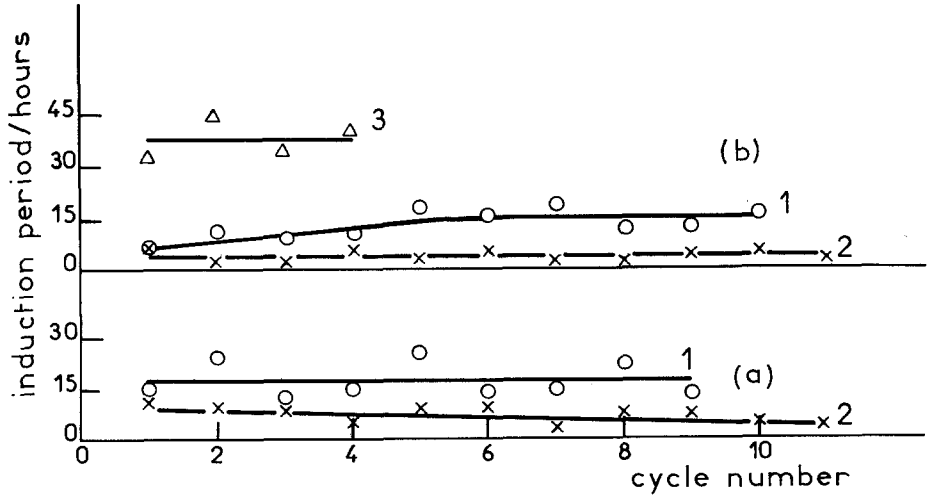

Fig. 2. Induction period versus cycle number for $i = 50$ mA cm^{-2}; (a) 30 mg dm^{-3} Ni^{2+}, pure Al cathode; (1) with diaphragm; (2) without diaphragm; (b) 5 mg dm^{-3} Ni^{2+}, RdH–Al cathode (○ and ×), pure Al cathode (Δ) (1) with diaphragm; (2) without diaphragm; (3) with diaphragm.

the induction period for a pure Al cathode fluctuates between 12 and 25 h, around a mean value of 17 h, with the diaphragm (curve 1). Under the same conditions but in the absence of the diaphragm, the induction period progressively decreases from 10 hours to 4 hours after 10 cycles (curve 2) and it even reaches 2.5 hours at cycle 20.

When using the RdH–Al cathode, the induction period is much lower than with pure Al, and falls to about 0.5 h under the conditions of Fig. 2(a), so that it becomes very difficult to observe a significant effect of diaphragm on the induction period. However, at a low Ni^{2+} concentration, 5 mg dm^{-3}, a similar effect of diaphragm is evident for the RdH–Al cathode (Fig. 2b): the induction period remains close to 4 h without the diaphragm (curve 2) whereas it increases with cycle number to stay about 15 hours after cycle 5 in the presence of the diaphragm (curve 1). In Fig. 2(b), it also appears that the RdH–Al cathode (curve 1) is characterized by a lower induction period than for pure Al (curve 3).

These results clearly show that the electrode destabilization by Ni^{2+} ions in the electrolyte is enhanced by anodically formed products. The absence of the diaphragm may favour interactions on the cathode between nickel and oxidized species, the anode potential being high enough ($\sim$ 1.3 V) to generate H_2O_2 or $S_2O_8^{2-}$ in the electrolyte. With the pure Al cathode, without the diaphragm (Fig. 2a, curve 2) the slow decrease of the induction period indicates that the surface concentration of impurities increases with electrolysis time. With the RdH–Al electrode the low values of the induction period imply a strong synergetic influence of nickel and oxidized species on the Fe aggregates included in the material (Fig. 2b, curve 2). The lower value of the induction period when the RdH–Al cathode is used with the presence of the diaphragm (Fig. 2b, curve 1) in comparison with the induction period for a pure Al cathode (Fig. 2b, curve 3) confirms the previously observed influence of the Fe aggregates included in the cathode material on the induction period [11].

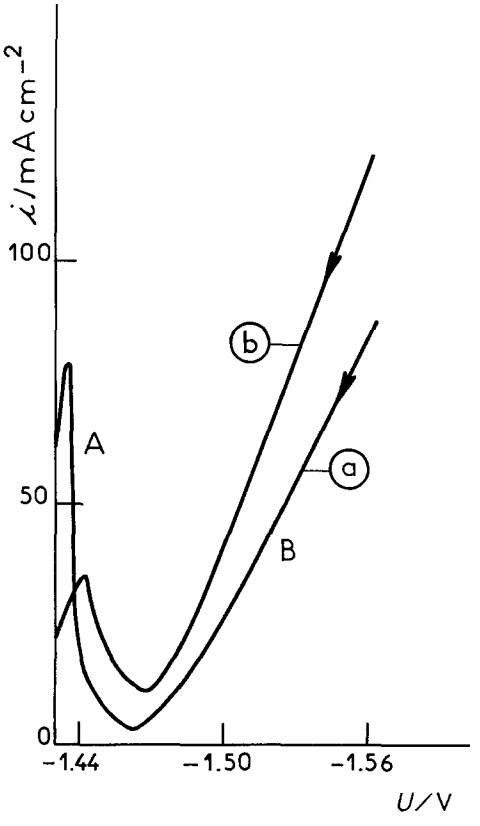

Fig. 3. Voltammograms recorded, at the sweep rate 3 mV s^{-1}, after maintaining U at −1.56 V for the time t. Pure Al cathode, electrolyte containing 30 mg dm^{-3} Ni^{2+}. (a) With diaphragm, t = 15.5 h, (b) without diaphragm, t = 1 h after cycle 10.

3.2. *Voltammetry*

The voltammograms recorded after maintaining the electrode potential, U, at −1.56 V for a given time also confirm the destabilizing influence of anodically formed products. Curve (a) in Fig. 3, obtained with the pure Al cathode and the presence of the diaphragm, shows a low value of the current minimum (at −1.46 V) which separates branch B, corresponding to zinc deposition, from the current peak A of hydrogen evolution. After only 1 h deposition from an electrolyte previously utilized during 10 cycles in the absence of the diaphragm (curve b), the current minimum is markedly increased and branch B is depolarized, thus indicating a more advanced destabilization process of zinc deposition [12].

In Fig. 4 relative to the RdH–Al cathode, the voltammogram obtained with the diaphragm reveals that the current minimum is similar to that of curve b in Fig. 3, indicating that the destabilization process is stimulated by the impurities contained in the substrate. In addition a second peak for hydrogen evolution appears in Fig. 4. for U = −1.39 V. Such a peak was previously observed at the initial stage of zinc deposition and it was ascribed to hydrogen evolution onto nickel adsorbed preferentially on iron impurities [11]. The existence of the peak in Fig. 4 suggests that the substrate impurities have not been covered by the zinc deposited for 1 h at U = −1.56 V and still stimulate the hydrogen evolution.

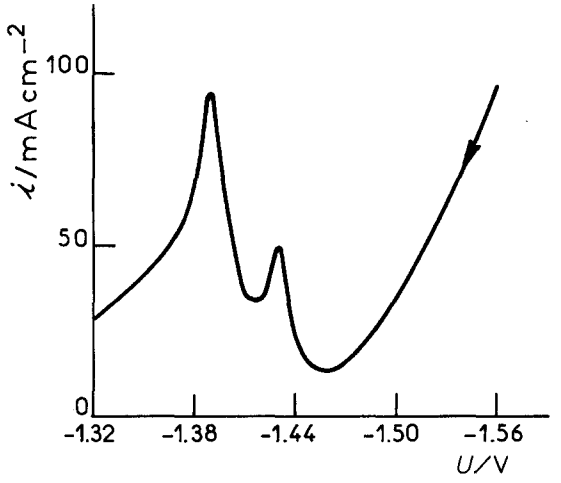

Fig. 4. Voltammogram recorded, at the sweep rate 3 mV s^{-1}, after maintaining U at −1.56 V for 1 h. RdH–Al cathode, Electrolyte containing 30 mg dm^{-3} Ni^{2+}, with diaphragm.

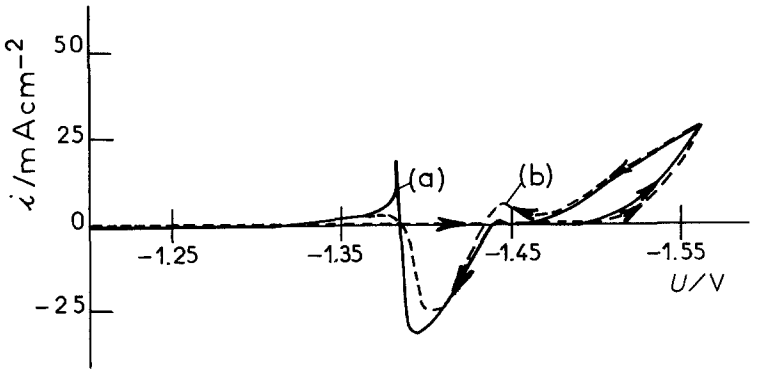

Fig. 5. Voltammograms recorded, at the sweep rate 3 mV s^{-1}, during the 4th scanning on a freshly polished cathode of pure aluminium. Electrolyte containing 30 mg dm^{-3} Ni^{2+} and previously used for 60 h. (a) With diaphragm, (b) without diaphragm.

The influence of anodically formed products also appears on voltammograms recorded at the beginning of electrolysis, precisely under conditions very sensitive to the presence of substrate impurities [11]. These experiments were conducted with freshly polished electrodes and a Ni^{2+}- containing electrolyte previously used for 60 h. At least four potential scans were necessary to reproduce stabilized voltammograms with the pure Al cathode in the whole potential range, except for the cathodic peak apparent at $U = -1.38$ V whose height was still increasing with scan number. The voltammograms obtained at the 4th scan are shown in Fig. 5. The slight current peak observed at $U = -1.44$ V on curve (a) with the diaphragm is considerably enhanced without the diaphragm (curve b). An opposite influence of diaphragm is observed on the peak at -1.38 V which is much less pronounced on curve b without the diaphragm.

Under the same potential sweep conditions, a different behaviour of the RdH–Al cathode has been observed, due to a much greater hydrogen evolution on the bare substrate, as evidenced from the peaks apparent in Fig. 6 at -1.38 V and around -1.4 V on the reverse and direct scans, respectively. At the 4th scan, the current is stabilized only for the reverse scan between -1.56 V and -1.4 V, and the cathodic peak at -1.38 V is still developing. However, it is clear that all peaks are stimulated (curve b) by the anodically formed products which interfere with Ni^{2+} ions at the cathode, in the absence of the diaphragm.

Thus a strong synergetic influence of nickel ions and oxidized species takes place on both Al substrates, enhancing the current peak at -1.44 V in both cases, and also the current peaks for the bare RdH–Al substrate.

3.3. *Impedance measurements*

Figure 7 shows two impedance plots obtained after electrolysis for time t, at a current density of 50 mA cm^{-2}. The steady-state electrode potential E was deduced from the stabilized potential, U, corrected for the ohmic drop, $R_e i$, due to the electrolyte resistance, R_e, given by the high-frequency limit of

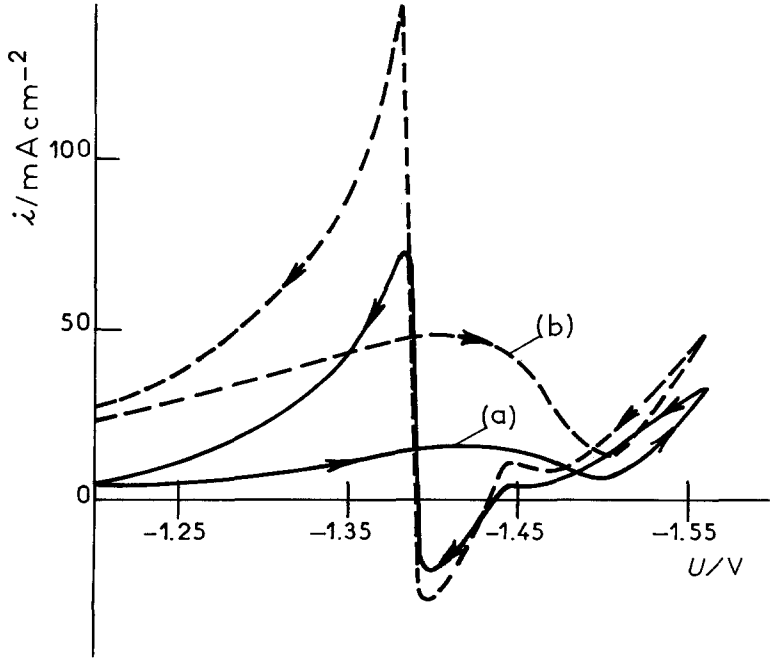

Fig. 6. Voltammograms recorded, at the sweep rate 3 mV s^{-1}, during the 4th scanning on a freshly polished cathode of RdH–Al. Electrolyte containing 30 mg dm^{-3} Ni^{2+} and previously used for 60 h. (a) With diaphragm, (b) without diaphragm.

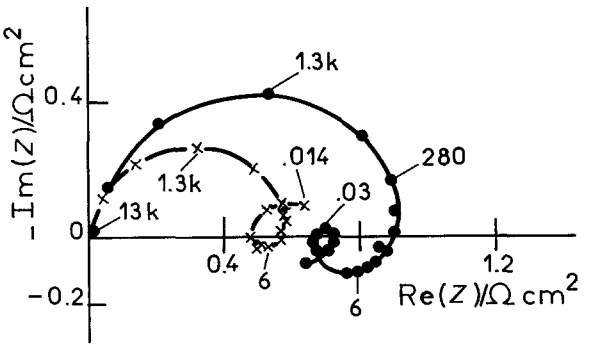

Fig. 7. Complex plane impedance plots obtained after the time t at $i = 50\,\text{mA cm}^{-2}$. Pure Al cathode, electrolyte containing $30\,\text{mg dm}^{-3}$ Ni^{2+}. (●) With diaphragm, $t = 6\,\text{h}$, $E = -1.524\,\text{V}$; (×) without diaphragm, $t = 2.5\,\text{h}$ after cycle 10, $E = -1.509\,\text{V}$.

the impedance. With no diaphragm, the charge transfer resistance, R_t, given by the size of the high-frequency capacitive loop, is considerably decreased, probably because of interactions between nickel ions and anodic products. In addition, it appears that the low-frequency capacitive loop is bigger under the influence of anodic products which interfere with the slow processes taking place at the cathode surface.

The low-frequency capacitive loop observed with the stationary electrode has been previously [12] ascribed to a partly diffusion-control of zinc deposition. This interpretation is consistent with the results obtained with a rotating disc electrode, as shown in Fig. 8. The polarization curves $i(E)$ have been obtained under steady-state conditions. Starting from $i = 120\,\text{mA cm}^{-2}$, the current was stepped down and the potential measured after stabilization, the influence of anodic products being eliminated in the presence of the diaphragm. The electrode rotation speed inhibits the deposition process (curve b), probably because of trace lead present in the electrolyte, as already reported [4]. This inhibition vanishes with increasing current density, in agreement with lead deposition under mass-transfer control [4], thus yielding a progressive electrode activation consistent with the low-frequency inductive loop apparent on plot (B).

The high-frequency phenomena are also modified with increasing electrolysis time, particularly the charge transfer resistance, R_t, with no diaphragm. Figure 9 shows that both R_t and the electrode polarization decrease with increasing time, the sudden electrode destabilization taking place after 7 hours. The R_t peak apparent at this time is correlated with the deposit dissolution, in conformity with the peak already observed in the potential domain corresponding to the transition between zinc deposition and hydrogen evolution [12, 14]. Similar phenomena have been observed during the successive cycles of deposition/dissolution of zinc and the induction time decreased with electrolyte ageing, in conformity with Fig. 2(a).

4. Conclusion

From galvanostatic potential–time curves, voltammograms and impedance measurements, it is shown that the destabilization of the steady-state conditions for zinc deposition by Ni^{2+} ions present in the electrolyte is considerably favoured in the absence of a diaphragm separating the anode and cathode compartments. The induction time prior to the potential destabilization decreases and the time dependence of voltammograms is more pronounced without a diaphragm. It is concluded that the deleterious influence of Ni^{2+} ions is enhanced by the presence of anodically formed products near the cathode.

Comparing a pure Al cathode to a Riedel–Al cathode, containing mainly Fe impurities, leads to

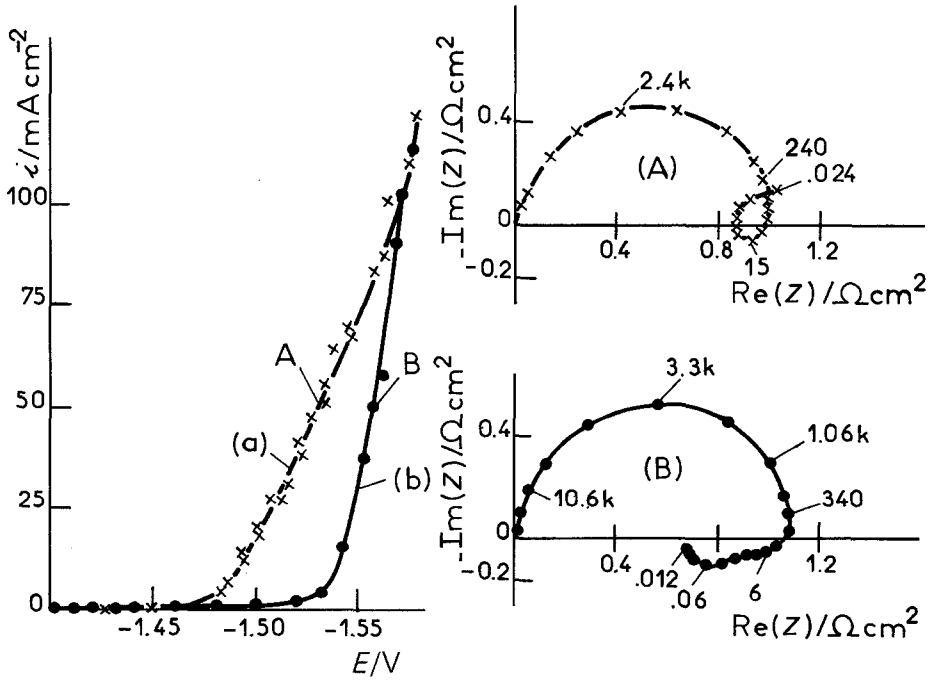

Fig. 8. Influence of the electrode rotation speed Ω observed in a nickel-free electrolyte, with diaphragm and pure Al cathode: (a) Ω = 0; (b) Ω = 2500 r.p.m. Complex plane impedance plots (A) and (B), at points A and B, respectively, on polarization curves, for $i = 50\,\text{mA cm}^{-2}$.

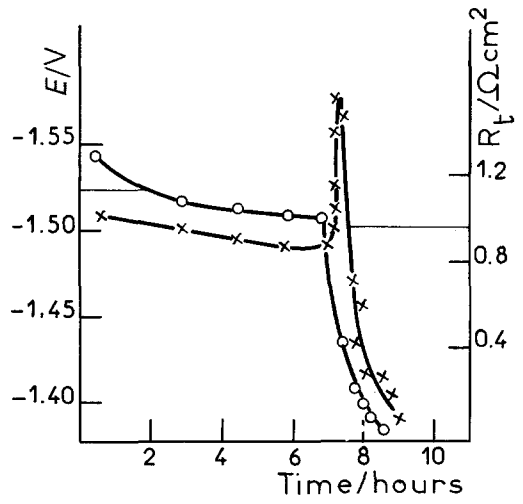

Fig. 9. Variation of the charge transfer resistance R_t (×) and electrode potential E (○) with electrolysis time. Electrolyte with 30 mg dm^{-3} Ni^{2+}. Pure Al cathode. Without diaphragm. Current density $i = 50$ mA cm^{-2}.

the conclusion that a strong synergetic influence of nickel and oxidized species takes place on the substrate impurities. Voltammograms suggest that the substrate impurities are hardly covered by the zinc deposit, thus maintaining a stimulated hydrogen evolution.

Impedance diagrams reveal a progressive decrease in charge transfer resistance during the induction time, and confirm that the anodic products interfere with the slow interfacial processes taking place at the cathode surface.

References

[1] R. C. Villas Boas, Synergetic phenomena in zinc electrowinning, NSF/CNPq, Rio de Janeiro, Brazil (1977).
[2] C. Cachet, B. Saidani and R. Wiart, *J. Electrochem. Soc.* **138** (1991) 678.
[3] D. J. Mackinnon and J. M. Brannen, *J. Appl. Electrochem.* **7** (1977) 451.
[4] E. J. Frazer, *J. Electrochem. Soc.* **135** (1988) 2465.
[5] D. J. Mackinnon, J. M. Brannen and R. C. Kerby, *J. Appl. Electrochem.* **9** (1979) 55.
[6] D. J. Mackinnon, J. M. Brannen and V. I. Lakshmanan, *ibid.* **9** (1979) 603.
[7] M. Maja, N. Penazzi, R. Frates and G. Roventi, *J. Electrochem. Soc.* **129** (1982) 2695.
[8] T. J. O'Keefe, S. F. Chen, E. R. Cole Jr and M. Dattilo, *J. Appl. Electrochem.* **16** (1986) 913.
[9] Y. M. Wang, T. J. O'Keefe and W. J. James, *J. Electrochem. Soc.* **127** (1980) 2589.
[10] D. J. Mackinnon and J. M. Brannen, *J. Appl. Electrochem.* **16** (1986) 127.
[11] C. Bozhkov, M. Petrova and S. Rashkov, *ibid.* **20** (1990) 11, 17.
[12] C. Cachet and R. Wiart, *ibid.* **20** (1990) 1009.
[13] *Idem*, The Electrochemical Society 182nd Meeting, Toronto, Canada, 11–16 Oct. (1992), Extended Abstracts Vol. 92–2, p. 544.
[14] R. Wiart, C. Cachet, C. Bozhkov and S. Rashkov, *J. Appl. Electrochem.* **20** (1990) 381.